Ribbon curling via stress relaxation in thin polymer films

Chris Prior[a], Julien Moussou[b], Buddhapriya Chakrabarti[a], Oliver E. Jensen[c], and Anne Juel[d,1]

[a]Department of Mathematical Sciences, Durham University, Durham DH1 3LE, United Kingdom; [b]Département de Physique, Ecole Normale Supérieure, 75005 Paris, France; [c]School of Mathematics, University of Manchester, Manchester M13 9PL, United Kingdom; and [d]Manchester Centre for Nonlinear Dynamics and School of Physics & Astronomy, University of Manchester, Manchester M13 9PL, United Kingdom

Edited by David A. Weitz, Harvard University, Cambridge, MA, and approved December 30, 2015 (received for review July 26, 2015)

The procedure of curling a ribbon by running it over a sharp blade is commonly used when wrapping presents. Despite its ubiquity, a quantitative explanation of this everyday phenomenon is still lacking. We address this using experiment and theory, examining the dependence of ribbon curvature on blade curvature, the longitudinal load imposed on the ribbon, and the speed of pulling. Experiments in which a ribbon is drawn steadily over a blade under a fixed load show that the ribbon curvature is generated over a restricted range of loads, the curvature/load relationship can be nonmonotonic, and faster pulling (under a constant imposed load) results in less tightly curled ribbons. We develop a theoretical model that captures these features, building on the concept that the ribbon under the imposed deformation undergoes differential plastic stretching across its thickness, resulting in a permanently curved shape. The model identifies factors that optimize curling and clarifies the physical mechanisms underlying the ribbon's nonlinear response to an apparently simple deformation.

elasticity | plasticity | yield | mechanics | stress relaxation

Bend a ribbon over a scissor blade by pressing it firmly down with your thumb and pull the ribbon over the blade. This is the commonplace method for curling ribbons for decorative gift wrapping. But what is the mechanism by which ribbon coils are produced? How does the coil depend on the speed of pulling, the shape of the blade, and the tension in the ribbon? We address these questions using a combination of experiments and theory, showing how curling arises via a plastic deformation that is regulated by both spatial and temporal effects.

A familiar example of curvature generation in thin materials is the bimetallic strip (or thermocouple), for which curvature arises from differential thermal expansion of two adherent layers of elastic material; the strip bends on heating but recovers its initially straight configuration on cooling to its original temperature (1). Some biological materials exploit the same principle, but with expansion driven by water fluxes: Reversible differential expansion arises in bilayer plant tissues such as the anther (2), pine cone scale (3), or wet paper (4), whereas irreversible differential cell expansion drives the bending of roots and shoots (5).

In contrast to these examples, a ribbon is a homogeneous material, at least before curling. Further, the curling deformation is permanent, pointing to the fact that a part of the material undergoes yield during the deformation process. Accordingly, the experiments we report below reveal that a threshold load must be applied to induce curling, whereas excessive loading may prevent curling or even tear the ribbon completely. Similar plastic deformation is inadvertently applied by rolling up paper scrolls for storage, resulting in curled edges that have plagued Chinese scrolls for centuries (6); however, the generation of this widthwise curvature is negligible in our narrow ribbons. Unlike prior studies of the bending of elastoplastic beams under a stationary transverse load (7, 8), our study addresses dynamic stress relaxation effects and shows how curling is modulated by an axial load. Our work also differs from studies of bending of soft viscoplastic threads, for which yield surfaces are orthogonal, rather than parallel, to the thread axis (9).

Somewhat surprisingly, our experiments show that the maximum ribbon curvature is typically generated at an intermediate load. We develop a theoretical model to explain the nonmonotonic relationship between curvature and load. The central idea is that as a material element of ribbon passes onto the blade and is forced into a configuration with high curvature it undergoes yield in a region near its outermost surface; however, as the ribbon element leaves the blade, there can be a further deformation involving irreversible stretching of the ribbon close to its inner surface. The former deformation promotes curling, and the latter reduces it. Curvature is modulated further by the pulling speed, which determines how the transit time of the element over the blade compares to the stress relaxation time of the material. Our model captures the key elements of this robust phenomenon and demonstrates how the curling process provides insight to the shear response of thin, stiff sheets of polymer that yield under relatively low loads.

Results

Experimental Results. A schematic side-view diagram of the experimental apparatus is shown in Fig. 1*A*. A polymer ribbon (10) of thickness $H^* = 100 \pm 3$ μm and width $W^* = 10.0 \pm 0.3$ mm, made from PVC transparency film, is pulled steadily over a blade at a prescribed rate (by attaching the ribbon to a rotating drum) and under a prescribed load (provided by a weight attached to one end). We used machined blades with radius of curvature $R^* = 1$, 1.5, and 2 mm and a fourth "sharp" blade with a much higher curvature ($R^* < 0.1$ mm). Pulling imprints a permanent curvature on the ribbon, which is measured after the ribbon is removed from the blade (Fig. 1*C*) (*SI Appendix*).

Images of the experimental ribbon configurations over each blade are shown in Fig. 1*B* for loads in the range 50 g $\leq m^* \leq$ 1,530 g. In

Significance

The forming of thin film structures through differential stress relaxation is an important engineering design tool to create flexible objects such as rolls, spirals, and origamis. We exploit the everyday process inspired from gift wrapping of curling an initially straight ribbon by pulling it over a blade to probe the mechanical shear response of thin polymer sheets. Experiments show that curling occurs over a limited range of loads applied to the ribbon, with the curl radius reaching a maximum at intermediate loads. A theoretical model reveals several patterns of irreversible yielding across the ribbon, and the dependence of curl radius on pulling speed shows that stress relaxes dynamically as the ribbon passes over the blade.

Author contributions: C.P., B.C., O.E.J., and A.J. designed research; C.P., J.M., B.C., O.E.J., and A.J. performed research; C.P., J.M., O.E.J., and A.J. analyzed data; and C.P., O.E.J., and A.J. wrote the paper.

The authors declare no conflict of interest.

This article is a PNAS Direct Submission.

[1]To whom correspondence should be addressed. Email: anne.juel@manchester.ac.uk.

This article contains supporting information online at www.pnas.org/lookup/suppl/doi:10.1073/pnas.1514626113/-/DCSupplemental.

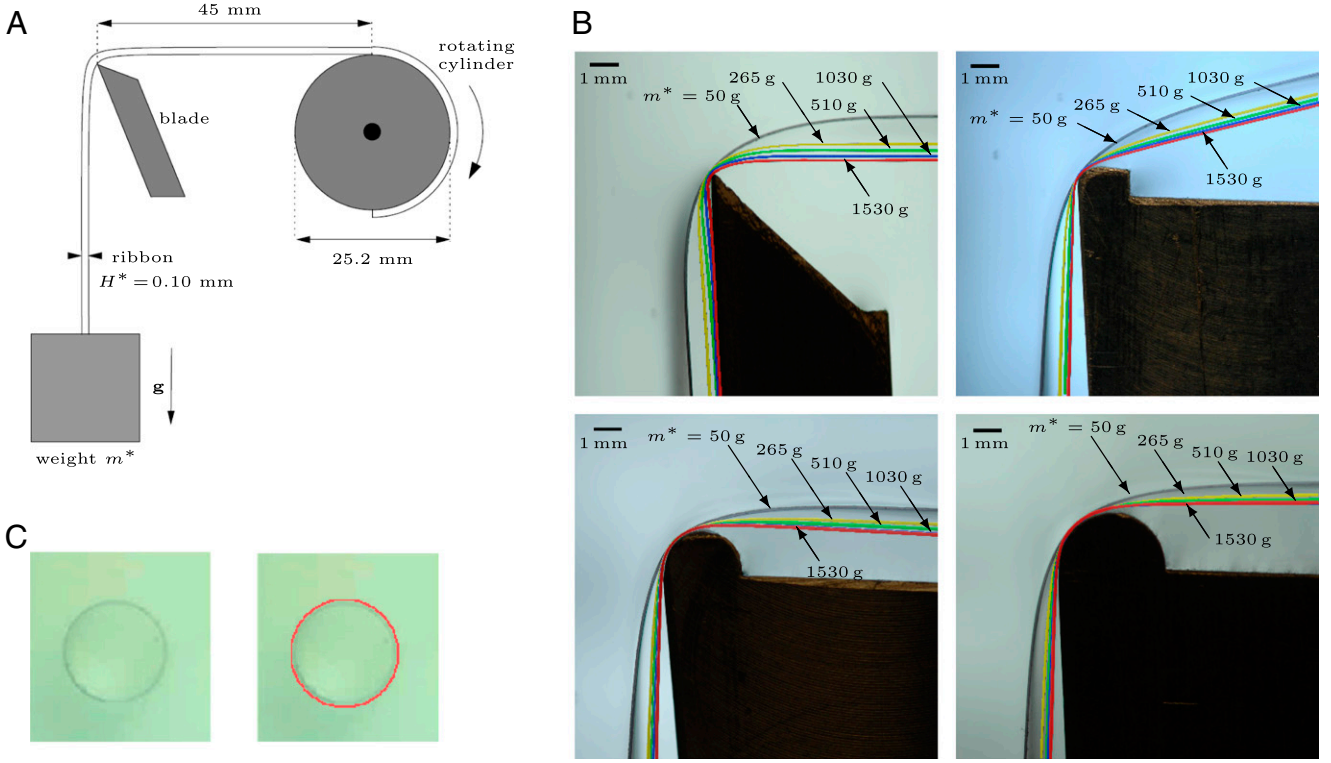

Fig. 1. Experimental setup for ribbon curling. (*A*) Side-view schematic diagram of the experimental apparatus. (*B*) Side-view photographs of the experimental ribbon shapes bending over the blade for different ribbon tensions imposed by hanging weights $m^* = 50$ g (gray), 265 g (yellow), 510 g (green), 1,030 g (blue), and 1,530 g (red) as shown in *A*. From top left to bottom right: sharp blade, blade radius $R^* = 1$ mm, $R^* = 1.5$ mm, and $R^* = 2$ mm. In all cases except for $R^* = 1$ mm, the rotating cylinder and top edge of the blade are positioned at the same height. For $R^* = 1$ mm (top right image), the cylinder position is higher than the blade so that the ribbon under tension is oriented with an angle of 14° with respect to the horizontal direction, and the contact area of the ribbon with the blade is reduced. (*C*) Measurement of the curl radius: top-view photograph of a single curl where the edge of the ribbon rests on a perspex sheet, and superposition of the ribbon outline obtained using edge-finding and the Hough transform onto the curled ribbon.

each case, the ribbon's resistance to bending led to slightly different ribbon geometries over the blade for increasing loads. This was most significant for the sharp blade where the ribbon configuration varied significantly over the entire range of loads and could not conform to the radius of curvature of the blade. Measurable changes in configuration were also found for the $R^* = 1$ mm blade over this range of loads; for $R^* = 1.5$ mm and $R^* = 2$ mm, the ribbon approximately adopted the curvature of the blade at $m^* = 1{,}030$ g and $m^* = 510$ g, respectively, so that the geometry of the ribbon remained unchanged for higher loads.

Dimensional permanent curvature measurements are shown using symbols in Fig. 2*A*, as a function of axial load applied to the ribbon for each of the four blades. The data corresponding to experiments with the sharp and $R^* = 1$ mm blades exhibit a characteristic triangular shape, where curvature increases approximately linearly with increasing load to a maximum in curvature that is larger the sharper the blade. The curvature then decreases monotonically upon further increase of the load. In both cases, the maximum load applied was determined by the smallest value of curvature that could be reliably measured at high loads. In contrast, for $R^* = 1.5$ mm and 2 mm, the curvature increased monotonically up to a maximum load, beyond which the ribbon ruptured. For $R^* = 1.5$ mm, the curvature seems to have reached a maximum, whereas for $R^* = 2$ mm only a small increase in curvature could be observed before the load exceeded its threshold value for rupture. The threshold load was found to increase as the curvature of the blade was reduced (Fig. 2*A*). The four sets of experimental data also suggest that a critical load needs to be exceeded in order for the ribbon to curl, and this critical load increases significantly with reduction in blade curvature. Hence, the modest loads required to bend the ribbon over the sharp and 1-mm blades meant that the ribbon geometry varied with load over the entire range investigated (Fig. 1*B*), whereas the larger loads required to bend the ribbon over the $R^* = 1.5$-mm and 2-mm blades exceeded the values at which the ribbon geometry reached a constant configuration. The effect on ribbon curling of the pulling speed was investigated for $R^* = 1$ mm and two applied loads ($m^* = 960$ and 689 g). Experimental data shown with symbols in Fig. 2*B* indicate that the curvature of the ribbon curl decreases monotonically with linear pulling speed.

To inform comparison with the theoretical model, the material properties of the PVC ribbon were measured with uniaxial tensile tests performed using an Instron 3345 (L2957) universal testing system. The Young's modulus E^* was determined by linear least-square fit of average stress-strain curves measured in the elastic regime to take a value of $E^* = 2.5 \pm 0.4$ GPa. The viscoplastic behavior of the material was investigated with creep experiments, where stress was applied to six different ribbon samples in successive step changes of variable magnitude. The average rate of plastic strain creep was determined with a linear fit to the time variation of strain data following each step change in applied stress. The average strain rate is shown in Fig. 2*C* as a function of applied stress, where each symbol indicates experiments performed on an individual ribbon sample. The strain rate is approximately zero below a critical yield stress and increases approximately linearly above this threshold. A linear fit to the data above the plastic yield threshold in Fig. 2*C* gave a viscosity coefficient of $\Phi^* = 92 \pm 4$ GPa·s, and extrapolation of the curve to zero average strain rate provided an estimate of a yield stress of

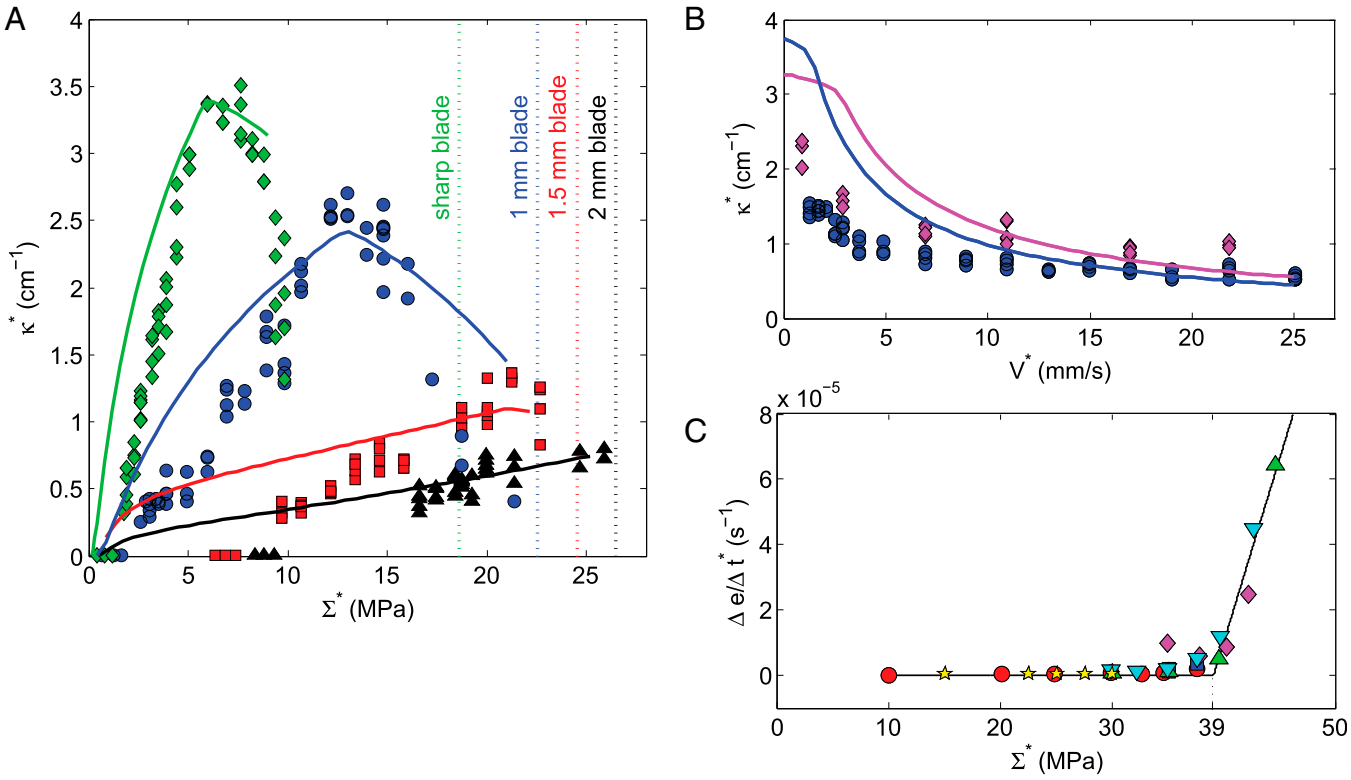

Fig. 2. Comparison between experimental measurements and theoretical predictions. (*A*) Symbols show experimental measurements of the permanent curvature of the curled ribbon as a function of stress applied to the end of the ribbon (see Fig. 1*A*) for the four blades: sharp blade (green diamond), $R^* = 1$ mm (blue circle), $R^* = 1.5$ mm (red square), and $R^* = 2$ mm (black triangle). In all cases, curling is observed above a threshold value of the applied load that depends on the radius of curvature of the blade. For the sharp blade, $R^* = 1$ mm and $R^* = 1.5$ mm, the curvature increases approximately linearly above the threshold load to a maximum value that decreases as R^* is increased. The curvature then decreases approximately linearly with applied load, and for $R^* = 1$ mm, the minimum values of curvature measurable experimentally are recovered. The vertical dotted lines correspond to the typical loads at which the ribbon ruptured on the blade. For $R^* = 1.5$ mm, the rupture load is very close to the maximum of curvature, so the decrease of curvature with load cannot be observed. For $R^* = 2$ mm, the curvature does not show evidence of a maximum below the rupture load. The pulling speed is $V^* = 4.9$ mm/s. Lines show model predictions using parameters $V^* = 4.9$ mm/s and $E^* = 2.5$ GPa. Values of the yield stress and plastic relaxation time were adjusted to $Y^* = 28$, 30, 31, and 40 MPa and $t_p^* = 0.15$, 0.18, 1.0, and 0.9 s for the sharp, 1-mm, 1.5-mm, and 2-mm blades, respectively. The angles at which the ribbon is pulled are similar to those shown in Fig. 1*B*. (*B*) Symbols show experimentally measured curvature as a function of pulling speed V^* for two different weights: $m^* = 689$ g (blue circles) and $m^* = 960$ g (magenta diamonds), using the blade with radius $R^* = 1$ mm. The curvature decreases approximately by a factor of three over the range of speeds investigated. Lines show model predictions using parameters for the 1-mm blade. (*C*) Average strain rate (symbols) measured as a function of applied stress during uniaxial tensile creep tests. A linear fit to the growing part of the curve (solid line) is extrapolated to zero strain rate to determine the yield stress $Y^* = 39$ MPa. Each type of symbol denotes a series of measurements performed on an individual ribbon sample. In each of these experiments, the imposed stress was incremented from zero in steps, and the strain was allowed to creep upward at each step until it reached an approximately constant value. An average strain rate was estimated at each step by a linear fit to the data.

$Y^* = 39 \pm 1$ MPa. However, as shown in Fig. 2*C*, small but measurable plastic strain rates were also found below this estimate of the yield stress for applied stress values larger than 32 MPa. Finally, tensile stress relaxation experiments performed by rapidly ramping the strain imposed on a sample ribbon to a fixed value and recording the reduction in stress that followed (*SI Appendix*) yielded maximum rates of plastic stress relaxation that increased weakly up to 1.8 MPa/s at 1.6% imposed strain and then more sharply and approximately linearly to 8 MPa/s for 4.4% imposed strain, relaxing to stresses in the range 28–36 MPa, with evidence of yield taking place even at strains below 1%. In summary, the ratio $Y^*/E^* \lesssim 0.016$ measured under extensional deformation indicates that the ribbon is a stiff material with a relatively low (but poorly defined) yield threshold, and estimates of stress relaxation time range from below 1 s to ∼40 s.

Physical Interpretation. Fig. 3 illustrates the mechanism that we propose to explain ribbon curling. The ribbon's complex constitutive properties are idealized by treating it as an isotropic elastic/viscoplastic material with a yield stress Y^* and a stress-relaxation timescale t_p^*, such that the material behaves elastically over timescales much less than t_p^* but stresses in excess of Y^* relax over a timescale t_p^* via irreversible deformation of the material; in line with experimental observations, we allow ourselves some latitude in defining precise values of Y^* and t_p^*. We ignore friction between the ribbon and the blade, so that the ribbon bears a uniform load along its length and remains isothermal. We consider the motion of an element of ribbon as it passes onto, over, and off the blade. In doing so, the curvature of the element (*i*) rises smoothly while the ribbon is off the blade, (*ii*) adopts the curvature of the blade while in contact with it, and then (*iii*–*v*) falls once off the blade (Fig. 3, *Top*), giving rise to stress distributions across the ribbon illustrated in Fig. 3 for low and high loads (cases A and B, respectively). Although the ribbon adopts a steady shape, material elements experience a time-varying curvature as they pass over the blade. The off-blade curvature distributions (*i* and *iii*–*v*) are regulated by a balance between the ribbon's bending resistance (which we assume is unaffected by any plastic deformation) and the imposed axial load. We assume that, as it passes over the blade, the ribbon element experiences a transverse strain gradient proportional to its

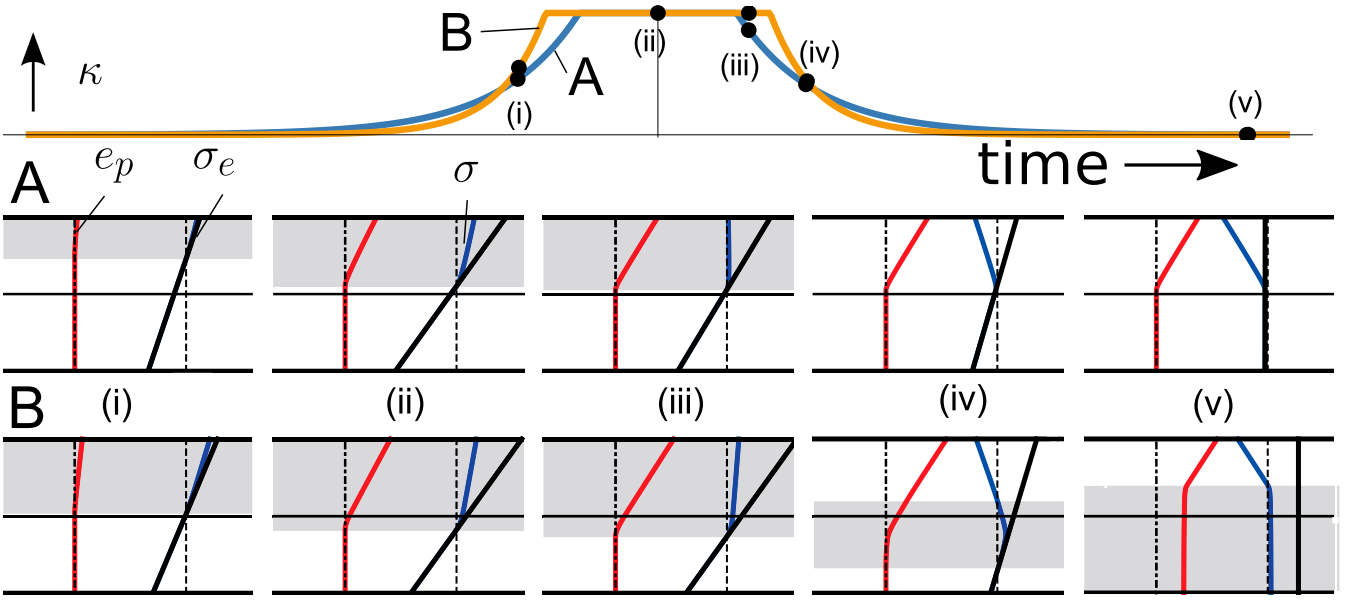

Fig. 3. Diagram illustrating the evolution of curvature, stress and plastic deformation of the ribbon for two parameter sets A and B, corresponding to the distinct regimes of behavior identified in the model. The parameters used in the calculations are $t_p^* = 0.35$ s, $Y^* = 35$ Mpa, $E^* = 2.5$ GPa, $H^* = 100$ μm, and $R^* = 1$ mm, with applied loads $\Sigma^* = 10$ MPa in A and $\Sigma^* = 30$ MPa in B. (*Top*) Depiction of the curvature κ of a material element of ribbon as a function of time as the element passes over the blade showing (*i*) preblade, (*ii*) on-blade, and (*iii–v*) postblade states. In these examples the ribbon comes into line contact with the blade, with its maximum curvature $1/R^*$ matching that of the blade. Increasing the axial load on the ribbon (going from A to B) reduces the lengthscale L_b^* over which the curvature decays off the blade and increases the width of the contact region. (*A* and *B*) Depictions of profiles across the ribbon cross-section of the axial stress distribution σ (blue) and the axial plastic strain e_p (red). Black lines show σ_e, the total axial strain times Young's modulus; its transverse gradient is determined by the instantaneous curvature of the ribbon element. The shaded regions indicate the yielding domain, denoting regions where σ exceeds the yield stress (indicated with a dashed line). In *i*, the increasing curvature raises σ above yield close to the outer surface of the ribbon; the material begins to relax, decreasing σ below σ_e and promoting a gradient in e_p. (*ii*) The stress integrated across the ribbon supports the constant imposed load, moving the yield surface toward the inner surface of the ribbon as the stress field relaxes. (*iii*) Just after leaving the blade, the yielded region is confined to the upper half of the ribbon under lower loads (*A*), but extends into the lower half of the ribbon under higher loads (*B*). (*iv*) The lowering curvature pivots the stress distribution around the ribbon midline: In *A* this lowers σ below the yield threshold, whereas in *B* the yielding region propagates further into the lower half of the ribbon. (*v*) As the ribbon element straightens, in *A* the final plastic strain is confined to the upper half of the ribbon, whereas in *B* the entire ribbon cross-section has undergone yield, leading to net axial stretch (see Movies S1 and S2).

instantaneous curvature, stretching the ribbon on its outer surface and compressing it (relatively) at its inner surface. Thus, upstream of the blade (*i*), the curvature-induced strain induces a transverse gradient of stress through an initial elastic response, which acts in addition to the axial loading on the ribbon. Where the stress exceeds Y^*, however, the ribbon starts to yield irreversibly (*i* and *ii* in Fig. 3); initially, this takes place close to the ribbon's outer surface. As the stress in the yielded region relaxes, the yielded region widens in order that the ribbon element can support a constant net axial load. Passing off the blade, the stress in the yielded region relaxes toward Y^*, leaving the ribbon irreversibly elongated at its outer surface (*iii* in Fig. 3).

Passage of the element further off the blade leads to a reduction in curvature and hence in the transverse strain gradient. Thus, via an initial elastic response, there is a corresponding reduction in the transverse stress gradient; this may be visualized as counterclockwise pivoting of the stress distribution about the ribbon's midline. If the yielded region remains confined to the upper half of the ribbon (*iv* and *v* in case A, Fig. 3), then no further yielding occurs. However, if the yielded region penetrates into the lower half of the ribbon, pivoting of the stress lowers the stress near the outer wall but creates a new zone near the ribbon's midline where the stress exceeds Y^*, (*iv* in case B, Fig. 3). This, in turn, induces a second phase of stress relaxation, involving widening of the central yielded region (*v* in case B, Fig. 3), and further irreversible elongation of the ribbon; this process is promoted by further curvature reduction as the ribbon element straightens out. Ultimately, the yielded region extends to the inner surface of the ribbon, reducing the gradient of irreversible strain. When unloaded, the curvature of the ribbon element is determined by the overall gradient of the net plastic strain; this gradient grows as the ribbon yields near its outer surface (*v* in case A, Fig. 3) but falls if there is additional yielding near the inner surface (*v* in case B, Fig. 3).

The minimal load required to induce a curl (Fig. 2*A*) can therefore be associated with the threshold required to induce yield at the ribbon's outer surface; the increase of curvature with load is associated with thickening of this yielded region (*i–iii* in case A, Fig. 3), and the reduction of curvature with load at higher load is due to the compensating yield near the inner surface (*iv* and *v* in case B, Fig. 3). The reduction of curvature with pulling speed (Fig. 2*B*) arises because the ribbon element has limited time in which to undergo stress relaxation while on the blade. Curling is maximized by driving the on-blade yield surface to the ribbon centerline (but not beyond), and by ensuring the ribbon moves slowly enough for the stress to relax fully before leaving the blade.

We can use experimentally measured parameters to estimate the load required to induce curling. We represent the load as an axial stress Σ^* and define the ratio of the ribbon's thickness H^* to the blade radius of curvature as $\epsilon \equiv H^*/R^*$, where $\epsilon \ll 1$. The ribbon will conform tightly to the blade if the bending length $L_b^* \equiv (E^* H^{*2}/\Sigma^*)^{1/2}$ (treating the ribbon as a loaded elastic beam) is small compared with R^*, that is, $\Sigma^* \gg \epsilon^2 E^*$. Preblade, we require $\Sigma^* < Y^*$ (to avoid large-scale yielding) and the mean axial strain is $O(\Sigma^*/E^*)$. The additional strain at the outer ribbon surface induced by curving the ribbon over the blade is $O(\epsilon)$, inducing an elastic stress $O(\epsilon E^*)$. For yielding to take place, we

therefore require Σ^* to lie in a window of width of order ϵE^* below Y^*. This explains why the threshold for curling is lower for sharper blades (Fig. 2*A*) but does not explain why the load leading to maximum curling falls for sharper blades. To address such questions, we now turn to a quantitative model, summarized briefly below and explained more fully in *Materials and Methods* and *SI Appendix*.

Model Predictions. Model predictions are shown using lines in Fig. 2*A*. The model predicts that curling takes place for loads satisfying

$$\Sigma^* > Y^* - \frac{1}{2}\kappa_{\max} E^*, \quad [1]$$

where the dimensionless curvature $\kappa_{\max}$ is the minimum of the curvature of the blade H^*/R^* (which arises at higher loads, when the ribbon is in line contact with the blade, as in Fig. 3*A*) and the maximum beam curvature $\sqrt{48\Sigma^*/E^*}$ (this arises at lower loads, when the ribbon is bent through 90° and in point contact with the blade).

The predicted ribbon curvature is composed of two curves, one rising with load and the second falling (Fig. 2*A*). On the rising curve, yield is confined to the upper half of the ribbon cross-section; on the falling curve, yield extends into the lower half of the cross-section. The threshold between the curves depends on geometric and material parameters and the speed at which the ribbon passes over the blade. Choosing values of Y^* and t_p^* (within the range of experimentally determined values) to match measurements of peak curvature, the model underestimates the minimum load for the onset of curling (although it provides a qualitative explanation for this behavior). Just as stress relaxation measurements reveal a range of yield stress values (*SI Appendix*), it was not possible to identify a single parameter set appropriate for all four blades, reflecting limitations of the constitutive model. The minimum load for curling is closely related to the assumed yield stress (see Eq. **1**); experimental data show that the sharp blade induces yielding at a lower effective yield stress, which is reflected by choosing a lower value of Y^*. Curling is promoted by allowing for full stress relaxation while the ribbon is on the blade. Because independent uniaxial tensile tests (*SI Appendix*, Fig. S1) show stress relaxation occurring more rapidly for larger strains, we adopt a smaller relaxation time for the experiments with sharper blades.

Lines on Fig. 2*B* show how the curvature is predicted to fall with increasing speed for a fixed load, using parameters for the 1-mm blade. The rate of decay of curvature with speed is captured reasonably well, and the model confirms that greater curvature may generally be achieved at lower speeds (and higher loads) by allowing for complete stress relaxation in the upper half of the ribbon. Although not evident in the experimental data, the model predicts that this effect may be offset at very low speeds (to the left of the kink in predicted curves), where the yield surface penetrates the lower half of the ribbon: In this case the model suggests that slightly greater curvatures can be achieved under lower loads.

The model predicts net axial elongation (in addition to curling) that undergoes a transition from modest to steep increase with load at approximately the load required for maximum curvature (Fig. 2*A*). Hence, net axial elongation is most significant along the falling part of the curvature–load curve. The experimental data confirm this prediction (*SI Appendix*, Fig. S2).

Discussion

Perhaps the most surprising feature of the experimental data reported here is the nonmonotonic dependence of curvature on load, showing that the applied load must be carefully tuned to maximize permanent ribbon curvature when using a blade of given radius. The load applied to the ribbon serves multiple purposes: It wraps the ribbon over the blade, forcing it to curve; it elevates the axial stress in the ribbon toward the yield stress; and it regulates the pattern of plastic deformation across the cross-section of the ribbon. When the ribbon is curved, stretching of the ribbon at its outer surface may be sufficient to induce plastic deformation locally. This deformation is applied to a length of ribbon by running the ribbon over the blade, at a speed that is sufficiently slow for part of the ribbon's cross-section to stretch irreversibly. If the stress relaxes while the ribbon is in a curved configuration, then straightening of the ribbon as it leaves the blade elevates the stress on the inner surface of the ribbon. If the load is sufficiently great, this can induce further plastic deformation, reducing the transverse strain gradients that lead to permanent curvature.

Experiments characterizing the material properties of the ribbon under elongation demonstrate surprisingly complex constitutive properties that we have not attempted to represent in full detail, choosing instead to work within the framework of a relatively simple (quasi-one-dimensional elastic–viscoplastic) constitutive model. Our semiquantitative predictions are sufficient to provide the physical insight needed to rationalize ribbon curling, during which extensional, shear, and viscous effects interact. Our model discounts frictional effects that may induce heating or surface deformations; these may contribute to curling in other circumstances.

The experimental protocol described here offers insights into material properties under shear of thin materials that are stiff but that yield at relatively low loads. The yield stress and relaxation time can be hard to define unambiguously for the polymer materials that often constitute ribbons, even in simple extensional tests. However, estimated geometric, material, and dynamic parameters (H^*/R^*, Y^*/E^* and $V^* t_p^*/R^*$) help define the range of loads over which curling arises and the tightness of the resulting curls.

Materials and Methods

Model Description. A full description of the mathematical derivation and solution of the model can be found in *SI Appendix*. The following highlights the model's key aspects.

To allow physical insight, our model seeks to capture the essential features of the experiment using a minimal number of parameters. We impose a strain field on a ribbon element as it moves from state to state and compute the resulting stress field. We calculate strain profiles by modeling the ribbon as an Euler–Bernoulli beam that is subject to an applied load and the constraint that it wraps around the blade for a portion of its length. This yields a curvature profile that is uniform on the blade and decays over a distance $L_b^* = (E^* H^{*2}/\Sigma^*)^{1/2}$ off it (Fig. 3, *Top*). The ribbon element experiences a transverse strain gradient, induced by the imposed curvature, superimposed on a transversely uniform axial strain. As shown in *SI Appendix*, the ribbon is found to be in point contact with the blade at low loads (when $L_b^* \geq \sqrt{48}R^*$, where the maximum curvature is $\sqrt{48}/L_b^*$); it is in point contact with maximum curvature $1/R^*$ for slightly higher loads and in line contact with maximum curvature $1/R^*$ for $L_b^* < R^*\sqrt{12(2-\sqrt{2})}$. Given a ribbon speed V^*, this yields the curvature history $\kappa^*(t^*)$ of a material element. Examples are shown in *SI Appendix*, Figs. S4–S6.

Given the imposed strain, we compute the stress by modeling the ribbon as a elastic/perfectly viscoplastic (Bingham–Maxwell) material, parametrized by a stiffness E^*, a yield stress Y^*, and a relaxation time t_p^*. We adopt a simplified representation for which the dominant stress and strain components in a ribbon element are purely axial and dependent on the transverse coordinate $H^* h$ (with $-1/2 < h < 1/2$), responding parametrically to changes in the element's curvature. Because we do not use a fully 3D formulation, we cannot expect estimates of the material parameters from unidirectional extensional deformations, which themselves show significant variability (Fig. 2*C* and *SI Appendix*), to transfer precisely to the more complex shear deformations associated with the curling experiment. Instead, we use the measured transit speed V^*, set $E^* = 2.5$ GPa (as measured) and adjust Y^* and t_p^* where they are used in the model within tightly defined ranges to fit the model to data. Having computed irreversible stretching of the ribbon element, its final curvature is computed by seeking its equilibrium configuration under zero load and moment.

To model plastic deformation, we nondimensionalize lengths by the ribbon thickness H^*, stresses by the yield stress Y^*, and time by $\pi R^*/2V^*$, the

time taken to pass over the blade. The dimensionless compliance parameter $\eta = Y^*/E^*$ is assumed small. In terms of the transverse coordinate h, directed from the inner to the outer wall of an element of ribbon, the axial strain distribution is assumed to take the form $e(h,t) = \overline{e}(t) + \kappa(t)h$, with $\overline{e}(t)$ the element's uniform stretch and $\kappa(t) = H^*\kappa^*$ the ribbon's centerline curvature. With $\kappa(t)$ prescribed, $\overline{e}(t)$ adjusts to accommodate plastic deformations. Before any plastic deformation, $\overline{e}(t) = \eta\Sigma$, where $\Sigma = \Sigma^*/Y^*$ represents the net axial load on the ribbon. We assume a linear-elastic/plastic strain decomposition $e(h,t) = \eta\sigma(h,t) + e_p(h,t)$, with σ the axial stress and e_p the plastic strain. The Bingham–Maxwell elastic/perfectly viscoplastic constitutive law (11) is

$$\frac{\mathrm{d}e}{\mathrm{d}t} \equiv \eta\frac{\mathrm{d}\sigma}{\mathrm{d}t} + \frac{\mathrm{d}e_p}{\mathrm{d}t} = \eta\frac{\mathrm{d}\sigma}{\mathrm{d}t} + \phi(\sigma-1)\,H_v(\sigma-1), \qquad [2]$$

where $\phi = \pi R^*\eta/(2V^*t_p^*)$ is an extensibility parameter and H_v the Heaviside function. We adopt a quasi-one-dimensional formulation, disregarding shear stresses so that h appears as a parameter in Eq. **2**; there is plastic deformation wherever $\sigma > 1$. The axial stress resultant balances the imposed load, giving

$$\int_{-1/2}^{1/2} \sigma(h,t)\mathrm{d}h = \Sigma. \qquad [3]$$

As shown in *SI Appendix*, this system can be reformulated as an integro-differential equation for e_p

$$\begin{aligned} \frac{\mathrm{d}e_p}{\mathrm{d}t} &= \frac{\phi}{\eta} f[e_p] H(f[e_p]), \\ f[e_p] &= \int_{-1/2}^{1/2} e_p \mathrm{d}h + \kappa h + \eta(\Sigma - 1) - e_p, \end{aligned} \qquad [4]$$

which was solved numerically up until a time at which the stress had fully relaxed. Once the load is removed from the ribbon, each element relaxes to form a coil with the ribbon's centerline having a constant equilibrium curvature κ_c and average strain $e_c = \overline{e}_c + \kappa_c h$. The blade-induced residual strain $e_p(h)$ means the stress in this state is $\sigma(h) = (e_c(h) - e_p(h))/\eta$, and we enforce force and moment balance under zero applied load and couple,

$$\int_{-1/2}^{1/2} \sigma \mathrm{d}h = 0, \text{ and } \int_{-1/2}^{1/2} h\sigma \mathrm{d}h = 0, \qquad [5]$$

to give $\overline{e}_c$ and κ_c.

Solutions of the numerical model are shown in Fig. 3 and *SI Appendix*, Figs. S7–S10. These are conveniently categorized by values of the dimensionless curling number, $\mathcal{C} \equiv H^*E^*/R^*Y^*$. When $\mathcal{C} < 2$, curling takes place in a narrow window of loads with the ribbon conforming tightly to the blade and the maximum equilibrium ribbon curvature is comparable in magnitude to that of the blade. The curvature of the ribbon at the lower threshold for curling is set by the blade, and the cutoff (Eq. **1**) lies at $(1 - (\mathcal{C}/2))Y^*$. For larger $\mathcal{C}$, the curling window extends to low loads [the load threshold being $O(H^*Y^*/R^*)$], encompassing (at the lowest loads) the case in which the ribbon bends gently over the blade. For sufficiently large $\mathcal{C}$, the resulting maximum equilibrium curvature is limited by the bending length of the ribbon to be of magnitude $1/(R^*\mathcal{C}) = Y^*/(H^*E^*)$ [i.e., $1/L_b^*$ with $E^*(H^*/L_b^*) = O(Y^*)$]. These estimates can be sharpened in the limit of rapid stress relaxation, when Eq. **4** can be simplified to yield an analytic approximation for the rising part of the curve relating equilibrium curvature κ_c and imposed load Σ, namely

$$\frac{\kappa_c}{\kappa_{\max}} = 1 + 2\left(\frac{2\eta(1-\Sigma)}{\kappa_{\max}}\right)^{3/2} - 3\left(\frac{2\eta(1-\Sigma)}{\kappa_{\max}}\right), \qquad [6]$$

where $\kappa_{\max} = \min(\epsilon, \sqrt{48\Sigma\eta})$, for $\kappa_{\max}/8 < \eta(1-\Sigma) < \kappa_{\max}/2$ (*SI Appendix* and *SI Appendix*, Fig. S11). In this limit the ribbon is predicted to be entirely in point contact with the blade for $\mathcal{C} > 8$, with maximum $\kappa^* = 4/\mathcal{C}R^*$, whereas for $\mathcal{C} < 8$ the maximum predicted curvature is $\kappa^* = 2/R^*$ with the ribbon in line contact with the blade. In practice, the ribbon curvature lies below these upper bounds if the on- or off-blade transit time falls beneath the stress-relaxation timescale, that is, for $V^*t_p^* \gtrsim \min(R^*, L_b^*)$.

ACKNOWLEDGMENTS. We thank H. Cass and A. Crowe for preliminary experiments, E. Häner for help with image analysis, and D. Pihler-Puzović for measurements of Young's modulus. B.C. thanks A. M. Klales; P. Hine for preliminary experiments; and V. Vitelli, V. N. Manoharan, and L. Mahadevan for preliminary discussions. We are grateful to a referee for valuable suggestions relating to our numerical solution scheme. This work was supported by an Addison–Wheeler Fellowship (to C.P.) and Engineering and Physical Sciences Research Council Grant EP/J007927/1.

1. Timoshenko SP (1925) Analysis of bi-metal thermostats. *J Opt Soc Am* 11: 233–255.
2. Nelson MR, et al. (2012) A biomechanical model of anther opening reveals the roles of dehydration and secondary thickening. *New Phytol* 196(4):1030–1037.
3. Reyssat E, Mahadevan L (2009) Hygromorphs: From pine cones to biomimetic bilayers. *J R Soc Interface* 6(39):951–957.
4. Reyssat E, Mahadevan L (2011) How wet paper curls. *EPL* 93:54001.
5. Moulia B, Fournier M (2009) The power and control of gravitropic movements in plants: A biomechanical and systems biology view. *J Exp Bot* 60(2): 461–486.
6. Chou M-H, Shen WC, Wang YP, Hung SH, Hong TM (2014) Curling edges: A problem that has plagued scrolls for millennia. *Phys Rev Lett* 112(3):034302.
7. Štok B, Halilovič M (2009) Analytic solutions in elasto-plastic bending of beams with rectangular cross section. *Appl Math Model* 33:1749–1760.
8. Kebadze E, Guest SD, Pellegrino S (2004) Bistable prestressed shell structures. *Int J Solids Struct* 41:2801–2820.
9. Balmforth NJ, Hewitt IJ (2013) Viscoplastic sheets and threads. *J Non-Newt Fluid Mech* 193:28–42.
10. Young RJ, Lovell PA (2011) *Introduction to Polymers* (CRC, Boca Raton, FL), 3rd Ed.
11. Lubliner J (2008) *Plasticity Theory* (Dover, Mineola, NY).